ARTICLE

Enhanced Photoelectric Conversion of Dye-sensitized Solar Cell by Addition of Inorganic Particles†

Bing Li, Ping Cheng, Chang-sheng Deng*

State Key Lab of New Ceramics and Fine Processing, Institute of Nuclear and New Energy Technology, Energy Science Building, Tsinghua University, Beijing 100084, China

(Dated: Received on August 30, 2007; Accepted on October 10, 2007)

Electrochemical impedance spectroscopy and cyclic voltammetry were used to investigate the effect of various inorganic particles, including titania, alumina, zirconia with particle sizes ranging from nano- to micro-meter on electrochemical properties of the electrolyte used in dye-sensitized solar cell. Adding inorganic particles could improve the ionic transport of I_3^- in the electrolyte and reduce the electrolyte-electrode transfer resistance, leading to an improvement of the photoelectric conversion efficiency of the devices. It was proposed that the improvement could be attributed to the interfacial effect between the inorganic particles and the electrolyte; ionic conduction paths formed between the solid particles facilitate the diffusion of the I_3^- in the electrolyte and improve the connection between the electrolyte and the electrode. Combined with a less volatile solvent system and a proper amount of the inorganic particles as the additive, an overall efficiency of 5.5% for the DSC (1 cm^2) with P25 (10%) under 100 mW/cm^2 at room temperature was achieved, an improvement of 51% over that without the oxide additive.

Key words: Dye-sensitized solar cell, Electrolyte, Oxide particles additive

I. INTRODUCTION

Dye-sensitized solar cell (DSC), with its potentially low fabrication cost, has attracted considerable interests in the past 17 years. DSC usually consists of three main components: a dye-covered nanocrystalline TiO_2 layer on a transparent conductive oxide (TCO)-coated glass substrate, an iodide/triiodide redox couple in an organic solvent, and a platinized TCO-coated glass substrate. The pores of the TiO_2 layer are filled with the electrolyte [1].

However, due to the evaporation and possible leakage of the conventional acetonitrile-based liquid electrolyte, a hermetic sealing proved necessary and remains a technical obstacle to the practical applications of DSCs. Therefore, efforts have been intensively made to seek for alternative electrolytes, which led to the development of hole-transfer all-solid electrolyte (CuI [2,3], CuSCN [4,5], NiO [6-8]), ionic conductive polymer-based electrolyte [9,10], and more recently, ionic liquid electrolytes [11-13]. There have been several reports that inorganic particles could enhance the ionic transport of electrolytes both for Li^+ battery [14,15] and DSC [16-20]. These enhancements have been originated from the interfacial effects of solid-solid electrolyte [21]. Bhattacharyya *et al.* in a study on the electrolyte for Li^+ battery found that adding SiO_2, Al_2O_3, and TiO_2 into liquid electrolyte solution of $LiClO_4$ led to formation of "soggy sand electrolytes" [22], which improved significantly the Li^+ ionic conductivity. It is noted that the electrolyte used in DSC is fundamentally different from that for Li^+ battery in that the diffusion of I_3^- is the limiting process of ionic conduction of the DSC electrolyte [23]. Furthermore, the photovoltaic performance of the devices prepared with solid electrolytes still remains relatively low compared with that prepared with the acetonitrile-based liquid electrolyte, possibly due to the poor interfacial charge transfer between the electrolyte and the electrodes [7]. Therefore, there is still a need to investigate approaches to improving the electrochemical properties of liquid electrolyte with alternative solvents much reduced volatility than the acetonitrile-based solvent and to illustrate the mechanism that leads to the improvement in the device performance.

In this work, we systematically studied the effects of various inorganic oxide particles with particle sizes covering nano- to micro-meter range, on the electrochemical properties of the liquid electrolyte and the photovoltaic performance of DSCs. Such studies could provide better selection for device materials.

II. EXPERIMENTS

A. Materials and device preparation

The liquid electrolyte was composed of 0.5 mol/L LiI, 0.05 mol/L I_2, 0.5 mol/L 4-ter-butylpyridine (TBP). A mixture solvent of ethylene carbonate (EC) and propylene carbonate (PC) with volatility much lower than acetonitrile was employed. For the preparation of the electrolyte with inorganic particles as additives, a predetermined amount of the inorganic particles was added into the liquid electrolyte respectively under constant

†Part of the special issue from "The 6th China International Conference on Nanoscience and Technology, Chengdu (2007)".

*Author to whom correspondence should be addressed. E-mail: changsheng@mail.tsinghua.edu.cn

TABLE I Particle size and specific surface area of added powders

Inorganic particle	Average diameter/μm	$S_{BET}/(m^2/g)$
P25 (nano-TiO_2)	0.050	12.78
Coarse TiO_2	0.497	4.06
ZrO_2	0.700	2.14
Al_2O_3	5.596	1.07

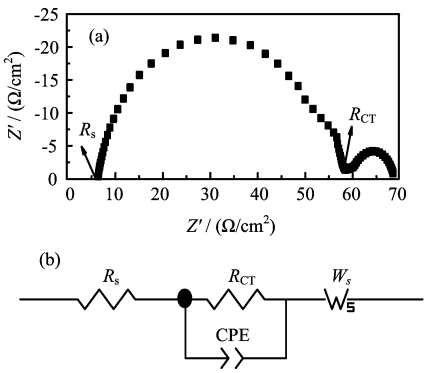

FIG. 1 (a) A typical impedance spectrum of liquid electrolyte; (b) Equivalent circuit for the impedance spectrum. R_s: Ohmic serial resistance. R_{CT}: Charge transfer resistance. W_s: Warburg impedance. CPE: Constant phase element.

stirring by sonification. Table I summarizes the average diameter and surface area of different inorganic particles used in this study.

B. Electrochemical measurements

Electrochemical impedance spectroscopy (EIS) was employed to analyze the electrolyte with a computer-controlled CHI604C model electrochemical workstation with a frequency range of 0.01-10^6 Hz. The magnitude of the alternative signal was 10 mV. The device for the EIS experiments consisted of two platinized electrodes, with the electrolyte filled in between. The impedance data was analyzed by using the ZVIEW software. The impedance spectra of the electrolyte with different inorganic particles were fitted using the equivalent circuit shown in Fig.1 [24]. The parameters for the circuit were optimized to ensure the best fit of experimental data.

The diffusion coefficient of I_3^- was determined using cyclic voltammetry (CV) on the device shown in Fig.1. The scan range was from −1.0 V to 1.0 V, and the scan rate was 10 mV/s.

C. Fabrication of DSCs and I-V measurement

Nanoporous TiO_2 films were manufactured by the well-documented procedures [1]. First a TiO_2 colloid was prepared by a hydrothermal method. Then the doctor blade technique was used to prepare a wet coating on a conducting glass sheet (FTO, Pilkington, TEC 15 Ω/□); finally the TiO_2 colloid film was sintered at 450 °C in air for 30 min to form nanocrystalline anatase structure. After cooled to 80 °C, the TiO_2 electrode was immersed in a 0.25 mmol/L *cis*-dithiocyanate-N,N'-bis(4,4'-dicarboxylate-2,2'-bipyridine)ruthenium(II) (N3, Solaronix) absolute ethanol solution for 12 h to chemically adsorb a monolayer of the dye, then the extra dye was washed away with anhydrous ethanol and the photoactive electrode was dried in air. A chemically platinized conductive glass with two holes was used as the counter electrode. Then the two electrodes were sealed by a polymer thin film, which also acted as a spacer for the electrolyte. Finally the liquid electrolyte dispersed with inorganic particles was injected into the cell through the holes on the counter electrode.

The photovoltaic characteristics of DSC were obtained by applying an external potential bias to the cell and measuring the generated photocurrent with a Keithley model 2400 digital source meter. A xenon lamp calibrated to 100 mW/cm^2 was used as the light source. The effective area was 1 cm^2 for all the dye solar cells.

III. RESULTS

A. Charge transfer resistance at electrolyte/Pt-FTO interface

The charge-transfer resistance R_{CT} associated with the heterogeneous electron exchange involving the electrolyte at the electrolyte/Pt-FTO interface is typically given for the equilibrium potential. The charge transfer resistance at electrolyte/Pt-FTO interface was extracted from EIS spectra and presented in Fig.2. Figure 2(a) shows the charge transfer resistance of the Pt/electrolyte interface as a function of the mass content of the oxide in the electrolyte. Addition of the oxide particles all led to an initial decrease of the charge transfer resistance from that of 55 Ω without oxide additive, and a minimum was reached at certain level of the oxide content, respectively. Further increase of the oxide load increased the charge transfer resistance. It is noted that there exists an order of charge transfer resistance for the electrolyte with addition of the oxide: Coarse TiO_2>P25>Al_2O_3>ZrO_2. The initial decrease in R_{CT} was more significant for P25, ZrO_2 than for Al_2O_3 and coarse TiO_2.

A diagram of the charge transfer resistance as a function of the total surface area per unit mass of the electrolyte was also presented in Fig.2. Despite of the large difference in the specific density of the added particles, the above observed trend of the charge transfer resistance still remains for individual oxide added electrolyte. The minimum charge transfer resistance was reached at 1.28, 0.81, 0.27, and 0.19 cm^2/g for P25, coarse TiO_2, ZrO_2, and Al_2O_3, respectively.

B. Diffusion coefficient of triiodide

Figure 3 shows a typical cyclic voltammegram of a liquid electrolyte with P25 particles used in DSCs, similar

DOI:10.1088/1674-0068/20/06/816-820

TABLE II I_3^- diffusion coefficient of quasi-solid electrolyte with different inorganic particles

P25			Coarse TiO_2			ZrO_2			Al_2O_3		
Content/%	S.A.	D	Content/%	S.A.	D	Content/%	S.A.	D	Content/%	S.A.	D
5	0.64	3.97	10	0.406	3.50	10	0.21	4.34	10	0.12	4.33
10	1.28	4.58	15	0.609	3.51	12.5	0.27	5.33	15	0.16	4.59
12.5	1.60	4.21	20	0.812	4.41	15	0.32	4.78	17.5	0.19	4.78
15	1.92	3.94	25	1.015	3.88	17.5	0.37	4.64	20	0.21	4.67
17.5	2.24	3.82	30	1.218	3.44	20	0.43	3.94	25	0.27	4.13

Note: S.A. is surface area, in cm^2/g, D in 10^6 cm^2/s.

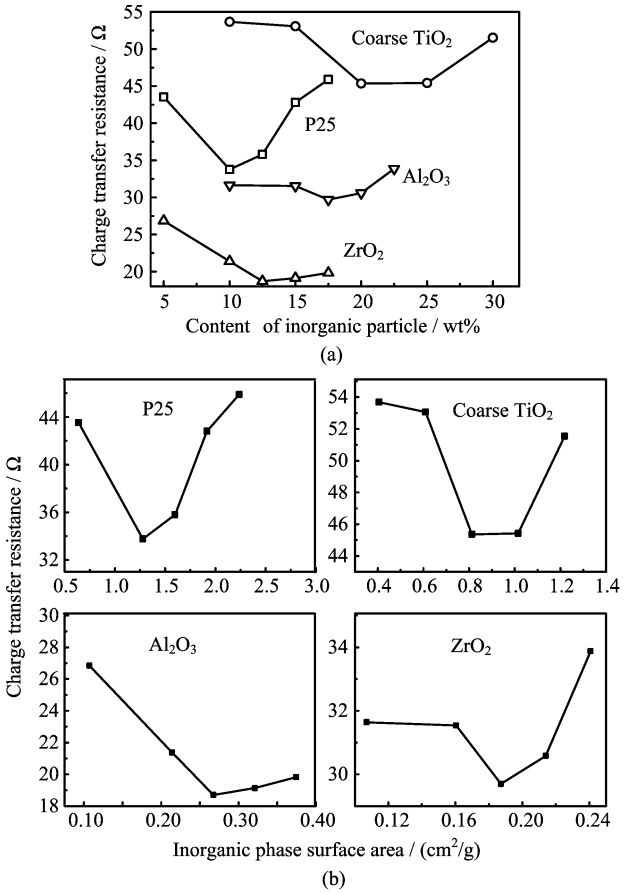

FIG. 2 Charge transfer resistance as a function of inorganic oxide particle content, and inorganic oxide particle surface area.

to that for a liquid electrolyte in principle. The resemblance between the anodic and cathodic limiting current ($j_{\rm lim}$) plateaus indicates steady-state conditions. Under this steady-state condition, the diffusion coefficient of triiodide $D_{I_3^-}$ can be calculated with the following formula [23,25]:

$$D_{I_3^-} = j_{\rm lim} l/2nFC_{I_3^-} \quad (1)$$

where n=2, indicating the electron-transfer number required for the reduction of I_3^-, $C_{I_3^-}$ is the bulk concentration of I_3^- (0.05 mol/L), l is the thickness of the thin layer cell (40 μm), and F is the Faraday constant. The triiodide diffusion coefficients of quasi-solid electrolyte containing different inorganic particle are summarized in Table II. The I_3^- diffusion coefficient for the electrolyte without oxide additives was 2.18×10^{-6} cm^2/s. With the increase of the inorganic oxide content, a trend reverse to the charge transfer resistance was observed for triiodide diffusion coefficient for all the inorganic oxide particles: an initial increase in D and attained maximum at certain point; upon further increase of the inorganic particles content, the diffusion coefficient decreased. The maximum diffusion coefficients are 4.58×10^{-6}, 4.41×10^{-6}, 4.76×10^{-6}, and 4.78×10^{-6} cm^2/s for electrolyte with contents of 10%, 20%, 15%, and 17.5% (mass), corresponding to surface area of 1.28, 0.81, 0.27, and 0.19 cm^2/g for P25, coarse TiO_2, ZrO_2 and Al_2O_3 as the additives, respectively. These diffusion coefficients were all more than two times that for the electrolyte without the oxide added.

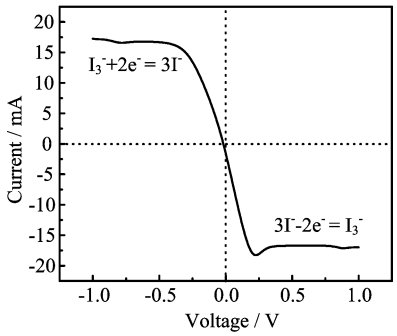

FIG. 3 Cyclic voltammegram of a typical liquid electrolyte with P25 added.

C. Photoelectric conversion efficiency of DSCs

The changes of the photo-electric conversion efficiency with the oxide content and oxide surface area, are presented in Fig.4. The photovoltaic conversion efficiency for the DSC with the electrolyte in the absence of oxide additive was 3.66%. Again, for all the DSCs, there is a maximum photo-electric conversion ef-

DOI:10.1088/1674-0068/20/06/816-820

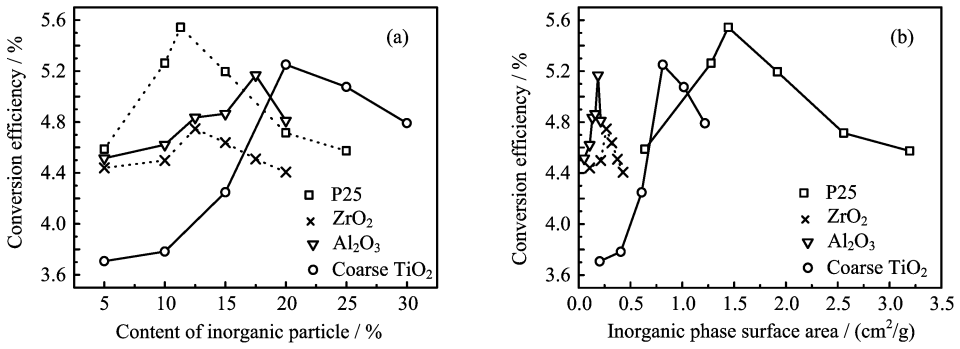

FIG. 4 Photo-electric conversion efficiency of the DSCs as a function of (a) oxide content and (b) oxide surface area.

ficiency with the oxide added into the liquid electrolyte. The maximum photo-electric conversion efficiencies are 5.54%, 5.25%, 4.75%, and 5.17%, an improvement of 51.4%, 43.4%, 29.8%, and 41.3% over the DSC without oxide, and corresponding to oxide surface area of 1.44, 0.81, 0.27, and 0.19 cm^2/g for P25, coarse TiO_2, ZrO_2, and Al_2O_3 added DSCs, respectively.

IV. DISCUSSION

The photovoltaic conversion efficiency of the DSCs with the oxide as additives exhibits significant improvement compared with those with liquid electrolytes at certain oxide load levels for all the oxide particles. This suggests that some unified mechanism is controlling such changes. Comparing the change in conversion efficiency with those of electrochemical properties of the electrolytes with oxide as the additives, one can see that there is a relatively good correlation in trend between the diffusion coefficient, the charge transfer resistance at electrolyte/Pt interface and the PV performance of the DSC devices, suggesting that the oxide additives significantly affect the photovoltaic conversion of the DSCs through their effects on the diffusion of I_3^- and the electrolyte/Pt interface charge transfer.

The ionic conductivity of the electrolyte $\sigma=ne\mu$, is related to the diffusion coefficient of the supporting electrolyte through Einstein's relation, $D=\mu kT$. In the two equations, n is the carrier density, μ the mobility, k Boltzmann constant and T the temperature [26].

Usually the short circuit current of DSC increases with the diffusion coefficient and open circuit voltage V_{OC} changes little [10]. For DSCs, Li^+, I^-, and I_3^- all contributed to the total ionic conduction. However, DSC performance is controlled by the ionic conduction of I_3^-, since I_3^- are the rate limiting species in the electrolyte. With the oxide added, two-fold effects were achieved. The I_3^- concentration was increased compared with the electrolyte in the absence of the oxide additives; also, the oxide particle surfaces assisted the ionic exchange reactions at the electrolyte/oxide interface region and at the electrolyte/Pt interface. These two effects work cooperatively to enhance the ionic conductivity of I_3^- in the electrolyte and the charge transfer at the electrolyte/Pt interface. Figure 5 shows schematically how the interfacial effect works on the ionic conduction in the electrolyte and at the electrolyte/Pt interface. Due to the surface acidic property, the inorganic particles can adsorb Li^+ on its surface (since the solvent is EC/PC, so the possibility that Li^+ be coordinated by N or O atoms as with acetonitrile as the solvent could be low), and then the Li^+ can attract counter ions I^- and I_3^-, forming ionic shells. The connection of the ions through these shells may form ionic exchange channels and connecting to the Pt electrode (I_3^- accepts electrons from Pt electrode), which provide easy pathways for the ionic conduction and charge exchange. It is immediately obvious that the greater the inorganic particles content, the more particles are connected, forming more domains of ion-exchange paths. The optimum point would be such that the ionic exchange effect for I^- and I_3^- in the electrolyte liquid and at the solid oxide/liquid interface reaches maximum, possibly when inorganic particles touch upon each other through the ionic outer shells

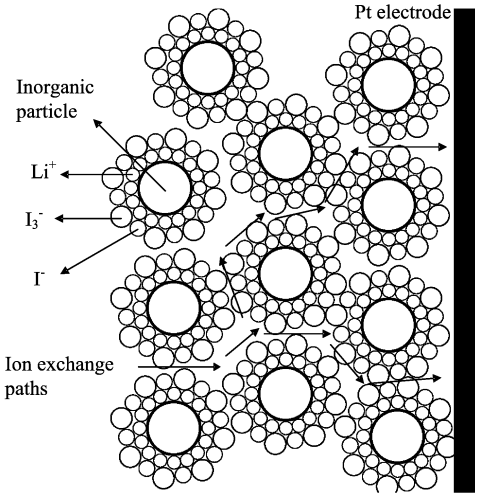

FIG. 5 Schematic diagram of ion conduction in liquid/inorganic-particle electrolyte.

DOI:10.1088/1674-0068/20/06/816-820

throughout the electrolyte mixture and also, more contact points are formed with the Pt electrode. Further increase in the particle contents would lead to increased tortuosity of the conduction paths, even to blockage of the paths, making the diffusion of triiodide difficult. The change in diffusion coefficients for different oxide additives is in accordance with the interfacial enhancement mechanism. The pH at zero charge (pzc) are 5, 7, and 8.5 for TiO_2, ZrO_2 and Al_2O_3, respectively. The diffusion coefficients for ZrO_2 and Al_2O_3 are larger than those for TiO_2 as the additives. Contrary to Li^+ conduction of the electrolyte for Li^+ battery [22], for the electrolytes studied here, the higher the pzc is, the less acidic the particle surface is, the lower ability to attract Li^+ ions is and, the lower the I_3^- diffusion coefficient is. This qualitatively explains the above results. Why the maximum diffusion coefficient for ZrO_2 is smaller than Al_2O_3 remains elusive to us at present. It is noted that the maximum photovoltaic conversion efficiencies for the DSCs do not follow exactly the above order, and careful examination indicates that the particle size of the added oxide also plays an important role. The maximum PV conversion efficiency was achieved with P25 as the additive. This might be attributed to that the electrolyte with larger oxide tends to have fewer particles penetrating into the nanoporous structure of the dye-sensitized TiO_2 electrode, which normally has pore sizes in the range of nanometers [27], consequently leading to e.g., partially blocking the nanopores in the electrode, and reducing the path cross-section of the electrolyte in the electrode, hence lowering short circuit current. *I-V* curves for the DSCs with maximum photoelectric conversion efficiency (not shown) indicate that I_{SC} for P25 is significantly larger than that for the other three oxides (the other three oxide all show very close I_{SC}), which all have particle sizes much larger than the pore size of the TiO_2 electrode.

V. CONCLUSION

Adding inorganic oxide particles TiO_2, Al_2O_3, and ZrO_2 to liquid electrolyte can improve the photo-electric conversion efficiency. DSCs with nanoparticles TiO_2 as the electrolyte additive had the highest photoelectric conversion efficiency of 5.5%, an improvement of 51.4% over that without oxide additives. Such improvement was resulted from the improved diffusion of I_3^- in the electrolyte and reduced charge transfer resistance at the electrolyte/Pt electrode. The particle size of the added oxide also has an important effect on the performance of the DSCs.

VI. ACKNOWLEDGMENT

This work was supported by the Chinese HI-tech program (No.2006AA03Z218).

[1] M. Grätzel and B. O'Regan, Nature **353**, 737 (1991).
[2] K. Tennakone, G. R. R. A. Kumara, A. R. Kumarasinghe, K. G. U. Wijayantha, and P. M. Sirimanne, Semicond Sci. Technol. **10**, 1689 (1995).
[3] K. Tennakone, V. P. S. Perera, and M. K. I. Senevirathna, Sol. Energy Mater. Sol. Cells **86**, 443 (2005).
[4] B. O'Regan and D. T. Schwartz, Chem. Mater. **7**, 1349 (1995).
[5] B. O'Regan, D. Schwartz, S. M. Nakeeruddin, and M. Grätzel, Adv. Mater. **12**, 1263 (2000).
[6] J. Bandara and H. Weerasinghe, Sol. Energy Mater. Sol. Cells **85**, 385 (2005).
[7] J. E. Kroeze, N. Hirata, L. Schmidt-Mende, C. Orizu, S. D. Ogier, K. Carr, M. Grätzel, and J. R. Durrant, Adv. Funct. Mater. **16**, 1832 (2006).
[8] C. Lévy-Clément, R. Tena-Zaera, M. A. Ryan, A. Katty, and G. Hodes, Adv. Mater. **17**, 1512 (2005).
[9] M. A. D. Paoli, C. Longo, and A. F. Nogueira, Coord. Chem. Rev. **248**, 1455 (2004).
[10] T. Asano, T. Kubo, and Y. Nishikitani, J. Photochem. Photobiol. A: Chem. **164**, 111 (2004).
[11] D. Kuang, C. Klein, S. Ito, J. E. Moser, R. Humphry-Baker, N. Evans, F. Duriaux, C. Grätzel, S. M. Zakeeruddin, and M. Grätzel, Adv. Mater. **19**, 1133 (2007).
[12] P. Wang, Q. Dai, S. M. Zakeeruddin, M. Forsyth, D. R. MacFarlane, and M. Gratzel, J. Am. Chem. Soc. **126**, 13590 (2004).
[13] P. Wang and M. Grätzel, Appl. Phys. Lett. **86**, 123508 (2005).
[14] F. Croce, G. B. Appetecchi, L. Persi, and B. Scrosati, Nature **394**, 456 (1998).
[15] C. W. Nan, L. Z. Fan, Y. H. Lin, and Q. Cai, Phys. Rev. Lett. **91**, 266104 (2003).
[16] H. Wang, H. Li, B. F. Xue, Z. X. Wang, Q. B. Meng, and L. Q Chen, J. Am. Chem. Soc. **127**, 6394 (2005).
[17] H. Yang, Z. G. Zhou, Z. G. Chen, F.Y. Li, T. Yi, and C. H. Huang, Chin. J. Chem. **24**, 1737 (2006).
[18] H. Usui, M. H., N. Tanabe, and S. Yanagida, J. Photochem. Photobiol. A: Chem. **164**, 97 (2004).
[19] E. Stathatos, L. R., S. M. Zakeeruddin, P. Liska, and M. Gratzel, Chem. Mater. **15**, 1825 (2003).
[20] G. S. T. Katsaros, I. M. Arabatzis, K. G. Papadokostaki, and P. Falaras, J. Photochem. Photobiol. A: Chem. **149**, 191 (2002).
[21] C. C. Liang, J. Electrochem. Soc. **120**, 1289 (1973).
[22] A. J. Bhattacharyya and J. Maier, Adv. Mater. **16**, 811 (2004).
[23] A. Hauch and A. Georg, Electrochim. Acta **46**, 3457 (2001).
[24] J. P. van de Lagemaat and N. G. Frank, J. Phys. Chem. B **104**, 2044 (2000).
[25] R. P. R. Greef, L. M. Peter, and D. Pletcher, J. Robinson, *Instrumental Methods Electrochemistry*, Chichester, England: Ellis Horwood Ltd., (1985).
[26] J. O. M. Bockris, A. K. N. R., *Modern Electrochemistry*, 2nd ed. Vol.1, New York: Plenum Press, 451 (1998).
[27] H. Arakawa, Z. S. Wang, and H. Kawauchi, Coord. Chem. Rev. **248**, 1381 (2004).

DOI:10.1088/1674-0068/20/06/816-820